MANUSCRIPT TITLE

Stable interaction of NONO with DBHS family members upon etoposide-induced DNA damage

AUTHORS

Barbara Trifault[1,2], Stephanie Lamer[3], Andreas Schlosser[3#], Kaspar Burger[1,2#*]

[1]Mildred Scheel Early Career Center for Cancer Research (Mildred-Scheel-Nachwuchszentrum, MSNZ) Würzburg, University Hospital Würzburg, Josef-Schneider-Str. 2, 97080 Würzburg, Germany.

[2]Department of Biochemistry and Molecular Biology, Biocenter of the University of Würzburg, Am Hubland, 97074 Würzburg, Germany.

[3]Rudolf-Virchow-Zentrum - Center for Integrative and Translational Bioimaging, University of Würzburg, Josef-Schneider-Str. 2, 97080 Würzburg, Germany

[#]equal contribution

*To whom correspondence should be addressed: E-mail: kaspar.burger@uni-wuerzburg.de (KB)

Short title

NONO interactome during DNA damage

ABSTRACT

The Non-POU domain containing octamer binding (NONO) protein is a member of the multifunctional *Drosophila* behavior/human splicing (DBHS) protein family and a core component of nuclear paraspeckles. NONO forms dimers with the other two DBHS members splicing factor proline and glutamine rich (SFPQ) protein or the paraspeckle component 1 (PSCP1) to modulate RNA metabolism and gene expression both at the transcriptional and post-transcriptional level. Increasing evidence suggests that NONO participates in genome maintenance by stimulating the DNA damage response (DDR) upon induction of DNA double-strand breaks (DSBs). However, the molecular principles that engage NONO in genome stability are poorly understood. We hypothesized that the induction of DSBs alters NONO protein-protein interactions and applied label-free mass spectrometry to test for changes in the interactome of NONO in human U2OS cells upon treatment with the topoisomerase II inhibitor etoposide. Surprisingly, our mass spectrometry data reveal that etoposide treatment does not induce major changes in NONO protein-protein interactions. We confirmed this finding by orthogonal co-immunoprecipitation assays and co-localization assays. Our data suggest that the bulk of interactions between NONO and SFPQ or PSPC1 are insensitive to etoposide treatment and that DBHS family members promote genome stability as stable dimers.

Keywords

DNA damage response; mass spectrometry; NONO; etoposide; DBHS proteins; nucleolus.

INTRODUCTION

RNA-binding proteins (RBPs) are an abundant protein family with critical roles in RNA metabolism. Utilizing a characteristic RNA recognition motif (RRM) and variable RNA-binding domains, RBPs recognize a diverse array of transcripts to participate in virtually all aspects of gene expression, ranging from the production and processing of nascent RNA in the nucleus to posttranscriptional roles in translation and RNA stability [1,2]. The Non-POU domain containing octamer binding (NONO) protein is a member of the *Drosophila* behavior/human splicing (DBHS) protein family and concentrates in paraspeckles. Paraspeckles are stress-responsive nuclear bodies that are built on the lncRNA NEAT1 and sequester 40 or so RBPs to form RNA metabolic hubs [3–7]. Members of the DBHS family are abundant and dynamic RBPs that mediate numerous protein-protein and protein-nucleic acid interactions to participate in various steps of pre-mRNA synthesis [8]. NONO self-dimerizes or forms heterodimers with the splicing factor proline and glutamine rich (SFPQ) protein or the paraspeckle component 1 (PSCP1) protein to promote the retention and editing of a subset of pre-mRNA transcripts within paraspeckles [9,10]. NONO also enriches on chromatin and associates with promoter-associated nascent transcripts to stimulate the formation of transcriptional condensates and augment RNA polymerase II activity [11–15]. First discovered as a splicing factor, NONO directly interacts with spliceosomal subunits and recognizes the 5' splice site, but is not essential for the splicing machinery in unperturbed cells [16,17]. Instead, NONO enhances pre-mRNA processing of super enhancer-associated transcripts upon oncogenic stress [18]. NONO is upregulated in many tumors and high levels of NONO foster the expression oncogenic transcriptional programs, which promotes proliferation and drug-resistance of cancer cells [19]. Thus, NONO is a multifunctional RNA metabolic factor.

Genome instability is a hallmark of cancer [20]. DNA double-strand breaks (DSBs) are highly toxic and threat genome stability [21,22]. To counteract genotoxic stress, the DNA

damage response (DDR) engages a myriad of proteins that sense and repair DSBs, including RBPs [23–25]. NONO and other DBHS family members are also linked to DDR and modulates the recognition and repair of DSBs [26]. Early studies suggest that NONO heterodimerizes with SFPQ to promote DSB pathway choice [27]. The depletion of NONO indeed delays the clearance of DSB foci and increases chromosomal aberrations [28,29]. NONO directly accumulates at DSBs and interacts with a subset of DDR factors, which fosters DSB repair via non-homologous end-joining (NHEJ) [30,31]. The accumulation of NONO at DSBs occurs in a poly(ADP-ribose)-dependent manner and involves the activation of the DSB-sensing DNA-dependent protein kinase (DNA-PK) [28,32]. More recently, novel mechanisms for the genome protective role of NONO have been reported, which include the relocalization of NONO and other DBHS family members to the nucleolus and nucleolus-associated condensates via interaction with nucleolar transcripts [33,34]. These findings underscore the relevance of NONO in promoting efficient DSB repair and genome stability.

Interestingly, NONO binding affinity to RNA substrates is regulated by the coactivator associated arginine methyltransferase 1 (CARM1/PRMT4) [35]. Moreover, NONO undergoes glycosylation and ubiquitinylation to efficiently accumulate at DSBs and UV-induced lesions, respectively [36,37]. However, to what extent DNA damage impacts on NONO protein-protein interactions is poorly understood. We hypothesized that the induction of DSBs alters the interactions of NONO with other DBHS family proteins and employed label-free quantitation by mass spectrometry to determine NONO protein-protein interactions in human U2OS cells in the absence or presence of the topoisomerase II inhibitor etoposide. Surprisingly, we observed no clear changes in the NONO interactome and persistent association of both SFPQ and PSPC1 to NONO. Persistent interaction of NONO with DBHS family members in response to etoposide treatment was validated by orthogonal assays and suggests remarkable stability of the bulk of *bona fide* NONO protein-protein interactions upon induction of DSB signaling.

95

96 **MATERIALS AND METHODS**

97 **Tissue culture, transfections, inhibitors and antibodies**

98 Human U2OS osteosarcoma cells were acquired from the German collection of microorganisms
99 and cell cultures (DSMZ), cultured at 37°C and 5 % CO2 in Dulbecco's modified eagle's
100 medium (DMEM, Gibco) complemented with 10 % fetal bovine serum (FBS, Capricorn), 100
101 U/mL penicillin-streptomycin (Gibco) and 2 mM L-glutamine (Gibco), and routinely tested for
102 mycoplasma infection. For ectopic expression, cells were transfected with 1.5 µg plasmid DNA
103 encoding HA-tagged NONO (pcDNA3.1-HA-NONO, kind gift from Nicolas Manel). For
104 knockdown experiments, cells were transfected with 100 nM siRNA that selectively targets
105 either NONO (siNONO, Dharmacon, L-007756-01 smart pool) or represents non-targeting
106 control (siControl, Dharmacon, D-001810-01 smart pool). Lipofectamine 2000 (Invitrogen)
107 and Opti-MEM (Gibco) was used for transfections according to the manufacturer´s protocol.
108 Incubation conditions with etoposide (Sigma) were for 2 h with 20 µM, unless stated
109 differently. The following antibodies were used in this study. Primary antibodies were: IgG
110 control (Proteintech, 30000-0-AP); NONO (Proteintech, 11058-1-AP); PSPC1 (Proteintech,
111 16714-1-AP); SFPQ (Abcam, ab177149); Ki-67 (Thermo, MA5-14520); HA-tag (Abcam,
112 ab9110; BioLegend, 901502); Fibrillarin (Abcam, ab5821); Vinculin (Sigma, V9131); histone
113 H2B (Abcam, ab1790); phospho-ser-139 histone H2A.X (Cell Signaling, 2577; Millipore, 05-
114 636); 53BP1 (Novus, NB100-304). Secondary antibodies were: HRP-linked IgG (Cytiva,
115 GEHENA934; Cytiva, NA931); Alexa Fluor 546-linked IgG (Thermo, A10036), Alexa Fluor
116 488-linked IgG (Thermo, A21206), Alexa Fluor 546-linked IgG (Thermo, A10040).

117

118 **Immunoblotting and immunoprecipitation**

119 Cells were lysed, boiled (5 min, 95°C) and sonicated (Branson, 10 %, 5 sec) in 4x sample buffer
120 (250 mM tris-HCl pH 6.8, 8 % sodium dodecyl sulphate (SDS), 40 % glycerol, 0.8 % β-
121 mercaptoethanol, 0.02 % bromophenol blue). Whole cell extracts were separated by
122 denaturating SDS polyacrylamide gel electrophoresis (PAGE) and transferred onto a
123 nitrocellulose membrane (Cytiva). Membranes were blocked (30 min, RT) in PBST (PBS/0.1
124 % triton x-100) with 5 % milk, probed with primary (overnight, 4°C) and secondary antibodies
125 (1 h, RT) diluted in PBST with or without milk and washed in between incubation steps with
126 PBST. Signals were visualized with an ECL kit (Cytiva) with an imaging station (Fusion FX
127 Vilber, LAS-4000 Fuji) and quantified with ImageJ (NIH). For immunoprecipitation, cells were
128 trypsinised, resuspended in DMEM, centrifuged (1200 rpm, 3 min), washed in cold PBS and
129 centrifuged again. The pellet was lysed for 10 min on ice in 5 volumes of IP buffer (200 mM
130 NaCl, 0.5 mM EDTA, 20 mM HEPES, 0.2 % NP-40, 10 % glycerol, 1x protease/phosphatase
131 inhibitor (Roche), 100 U of Ribolock RNase inhibitor (Thermo). Lysates were centrifuged
132 (12000 rpm, 12 min) and supernatants were collected in a new tube. 10 % of lysate was kept as
133 input (IN) and the remaining 90 % was incubated (3 h, 4°C) on a rotative wheel with 5 µg
134 primary antibody pre-conjugated with 30 µL G beads overnight. Crosslinking of pre-conjugated
135 antibodies was performed with bis(sulfosuccinimidyl)suberate (BS3, Thermo) or dimethyl
136 pimelimidate (DMP, Thermo) according to the manufacturer's protocol. Immunocomplexes
137 were captured on a magnet (Invitrogen), washed three times with 800 µL IP buffer and eluted
138 (5 min, 95°C) with 40 µL of 4x sample buffer (reducing condition). For native PAGE, samples
139 were eluted in 4x sample buffer without β-mercaptoethanol (non-reducing condition). Proteins
140 were visualized by using either a SilverQuest staining kit (Thermo) according to the
141 manufacturer´s protocol prior to transfer or by staining for 5 min at RT with Ponceau solution
142 (0.5 % Ponceau S/1 % acetic acid) after the transfer.
143

144 **Confocal imaging**

145 Cells grown on cover slips (Roth) were washed in PBS, fixed (10 min, RT) with 3 %
146 paraformaldehyde (Sigma), permeabilized (10 min, RT) with PBST, washed (5 min, three
147 times) in PBS and blocked (2 h, 4°C) with PBS/10 % FBS. For staining, cells were incubated
148 in a humidified chamber with primary antibodies (overnight at 4°C) and secondary antibodies
149 (2 h, RT) diluted in PBS/0.15 % FBS and secondary antibodies. Cells were washed with PBST
150 (three times, 5 min) between incubations and sealed in 4,6-diamidino-2-phenylindole (DAPI)-
151 containing mounting medium (Vectashield). Signals were imaged with a confocal microscope
152 (CLSM-Leica-SP2, x63 objective, 1024x1024 resolution, airy = 1) and channels were acquired
153 sequentially, between frames, with equal exposure times as single scans. Images were analyzed
154 and co-localization was assessed by ImageJ and RGB profiler (NIH).

155

156 **Nanoscale liquid chromatography coupled to tandem mass spectrometry (Nano LC-**
157 **MS/MS)**

158 For in-gel digestion, immunoselected proteins were eluted with 4x lithium dodecyl sulphate
159 (LDS) sample buffer (NuPAGE, Thermo) according to the manufacturer's protocol and
160 precipitated in a four-fold volume of acetone (overnight, -20°C). Precipitated proteins were
161 washed three times with acetone at -20°C, dissolved in 4x LDS sample buffer, reduced (10 min,
162 70°C) with 50 mM DTT and alkylated (20 min, RT) with 120 mM iodoacetamide. Proteins
163 were separated by Novex 4-12 % bis-tris gels with MOPS buffer (NuPAGE, Thermo) according
164 to the manufacturer's protocol. Gels were washed (5 min, three times) with ultrapure water,
165 stained (60 min, RT) with Coomassie (Thermo) and washed again for 1 h. All gel lanes were
166 cut in 15 slices, destained with 30 % acetonitrile in 0.1 M NH_4HCO_3 pH 8.0, shrunk with 100
167 % acetonitrile, and dried in a vacuum concentrator. Each gel band was digested (overnight,
168 37°C) with 0.1 µg trypsin in 0.1 M NH_4HCO_3 pH 8.0, the supernatant was removed and the

169 peptides were extracted from the gel slices with 5 % formic acid. The extracted peptides were
170 pooled with the supernatant. For NanoLC-MS/MS analysis, an Orbitrap Fusion (Thermo)
171 equipped with a PicoView Ion Source and coupled to an EASY-nLC 1000 was used. Peptides
172 were loaded on capillary columns (PicoFrit, 30 cm x 150 µm ID, New Objective) self-packed
173 with ReproSil-Pur 120 C18-AQ, 1.9 µm (Dr. Maisch) and separated with a linear gradient from
174 3 % to 30 % acetonitrile and 0.1 % formic acid (30 min, flow rate 500 nL/min). Scans were
175 acquired with a resolution of 7500 for MS/MS scans and 60000 for MS scans in the Orbitrap
176 analyzer. HCD fragmentation with 35 % normalized collision energy was applied and a top
177 speed data-dependent MS/MS method with a fixed cycle time of 3 sec was used. Dynamic
178 exclusion was set with a repeat count of 1 and an 30sec exclusion duration and singly charged
179 precursors were excluded from selection. Minimum signal threshold for precursor selection was
180 set to 5x104 and predictive AGC was used with a AGC target value of 2x105 for MS scans and
181 5x104 for MS/MS scans. EASY-IC was used for internal calibration.
182
183 **Mass spectrometry data analysis**
184 Raw MS data files were analyzed with MaxQuant version 1.6.2.2 [38]. Database search was
185 performed with Andromeda, which is integrated in the utilized version of MaxQuant. The
186 search was performed against the UniProt Human Reference Proteome database (January 2021,
187 UP000005640, 75777 entries). Additionally, a database containing common contaminants was
188 used. The search was performed with tryptic cleavage specificity with 3 allowed miscleavages.
189 Protein identification was monitored by setting a false-discovery rate (FDR) of <1 % on protein
190 and peptide spectrum match level. In addition to MaxQuant default settings, the search was
191 performed against the following variable modifications: Protein N-terminal acetylation, Gln to
192 pyro-Glu formation (N-term. Gln) and oxidation (Met). Carbamidomethyl (Cys) was set as
193 fixed modification. Further data analysis was performed using R scripts developed in-house.

194 LFQ intensities were used for protein quantitation [39]. Proteins with less than two razor/unique
195 peptides were removed. Missing LFQ intensities were imputed with values close to the baseline.
196 Data imputation was performed with values from a standard normal distribution with a mean
197 of the 5 % quantile of the combined log10-transformed LFQ intensities and a standard deviation
198 of 0.1. For the identification of significantly enriched proteins, median log2 transformed protein
199 ratios were calculated from the two replicate experiments and boxplot outliers were identified
200 in intensity bins of at least 300 proteins. Log2 transformed protein ratios of sample versus
201 control with values outside a 1.5x (significance 1) or 3x (significance 2) interquartile range
202 (IQR), respectively, were considered as significantly enriched in the individual replicates.
203

204 **Ethics statement**

205 All data are derived from the U2OS cancer cell line (non-pathogenic, non-infectious, safety
206 level S1), which has been isolated in 1964. U2OS cells are an established cancer model cell line
207 for more than 50 years and working with U2OS cells does not require ethical approval.
208

209 **RESULTS**

210 **Validation of NONO antibody from mass spectrometry**

211 We wished to study the impact of DNA damage on the NONO interactome in U2OS cells. We
212 acquired a knockout-validated polyclonal NONO antibody and confirmed its selectivity upon
213 RNAi-mediated depletion of NONO. Using the NONO antibody for immunoblotting and
214 immunofluorescence microscopy, we observed prominent reduction in reactivity upon
215 transfection of NONO-selective siRNA (Fig. S1A-C). Next, we validated the induction of DNA
216 damage by confocal imaging of DSB markers in response to etoposide treatment. As expected,
217 we observed prominent formation of nuclear foci in the presence of etoposide that stained
218 positive for the *bona fide* DSB marker p53-binding protein 1 (53BP1) and partially overlapped

219 with signals for the DNA damage marker serine-139 phosphorylated histone H2A.X variant
220 (γH2A.X) (Fig. S1D and E). We also tested the capacity of the antibody to immunoselect
221 NONO and performed immunoprecipitation experiments (Fig. S1F). Indeed, the antibody
222 efficiently enriched NONO from U2OS whole cell lysates, irrespective of etoposide treatment
223 conditions. Thus, we established conditions to detect and immunoselect NONO in the absence
224 and presence of DSBs.

225 We noticed prominent immunoglobulins signals in our immunoprecipitation samples,
226 suggesting prominent coelution of bead-conjugated immunoglobulins. Excessive amounts of
227 immunoglobulins can perturb mass spectrometry data and prevent the detection of less abundant
228 peptides. Thus, aimed to covalently bind the antibody to the matrix and prevent coelution. We
229 elaborated on our immunoprecipitation protocol and introduced a crosslinking step using either
230 BS3 or DMP reagent (Fig. S1G). Using non-reducing conditions, we found that both BS3 and
231 DMP efficiently prevented coelution of immunoglobulins from the beads. However, the NONO
232 antibody only tolerated BS3, but not DMP crosslinking and the latter prevented the efficient
233 immunoselection of NONO from lysates. We repeated the immunoprecipitation experiment and
234 assessed NONO levels after either non-reducing or reducing separation conditions (Fig. S1H).
235 Immunoblotting for NONO confirmed that BS3 crosslinking both preserves the affinity of the
236 antibody toward NONO and prevents coelution of immunoglobulins from the beads. We
237 conclude that etoposide treatment and antibody crosslinking by BS3 are appropriate to assess
238 changes in the NONO interactome upon DNA damage.

239

240 **Persistent interaction of NONO with DBHS family members upon DNA damage**

241 Having established conditions to immunoselect NONO, we applied mass spectrometry to
242 determine the impact of DNA damage on NONO protein-protein interactions. For comparative
243 analysis of two biological replicates, we incubated cells in the absence or presence of DNA

244 damage and performed immunoprecipitation from whole cell lysates using either the NONO
245 antibody or an isotype control (Fig. S2A). Correlation analysis revealed a high similarity
246 between replicates, irrespective of the antibody used for immunoprecipitation or etoposide
247 treatment (Fig. S2B). Overall, we detected 1031 proteins that were reproducibly present upon
248 NONO immunoprecipitation, albeit many of them with low peptide counts or poor sequence
249 coverage. To increase stringency, we considered only those as hits that were detected by at least
250 five unique peptides in the NONO immunoprecipitation samples. Such filtering narrowed down
251 the list of proteins to 238 that were immunoselected by the NONO antibody in the absence or
252 presence of etoposide treatment (Fig. 1A). Reassuringly, NONO was found as top hit together
253 with SFPQ and PSPC1, and all three DBHS family members scored with high significance
254 (Table S1). However, visual inspection of mass spectrometry data suggested an overall high
255 similarity between control and DNA damage conditions. Indeed, a stable, etoposide-resistant
256 interaction between NONO and DBHS family members was confirmed by immunoblotting
257 (Fig. 1B and C). Also, 76 of the top100 mass spectrometry hits were found in both conditions
258 (Fig. 1D; Table S2). To directly assess for differential co-enrichment of proteins in the absence
259 or presence of DNA damage, we integrated both treatment conditions into one graph (Fig. 2A).
260 Linear regression analysis revealed that PSPC1, SFPQ and virtually all other hits were co-
261 immunoprecipitated with NONO irrespective of etoposide treatment. We considered a second
262 filter and scored only those factors as significant that were at least 4-fold enriched over the
263 isotype control. This analysis yielded 49 proteins, out of which 28 were reported as nuclear
264 proteins. With a few exceptions, the list of top30 proteins is strikingly similar and the bulk of
265 filtered hits in the control condition are also found upon etoposide treatment (Fig. 2B). Of note,
266 90% or so of hits scoring as nuclear proteins were RBPs (Fig. S2C) and these included several
267 previously reported components of paraspeckles and NEAT1 interactors, such as HNRNPUL1,
268 YBX1 or SYNCRIP [40,41]. We conclude that our NONO interactome data are valid, but may

269 suffer from a considerable number of false-positive hits and cytoplasmic contaminants.
270 Surprisingly, the comparative analysis of NONO interactomes revealed no significant changes
271 in response to DNA damage.
272
273 **Co-localization of DBHS family members *in vivo* and concomitant nucleolar re-**
274 **localization upon DNA damage**
275 We could previously show that NONO, SFPQ and PSPC1 undergo nucleolar re-localization
276 upon etoposide treatment [34,42]. To corroborate our biochemical data and further assess the
277 association of NONO with DBHS family members in response to DNA damage *in vivo*, we
278 investigated the subcellular localization of DBHS proteins in the absence and presence of
279 etoposide by confocal imaging. We aimed to co-stain endogenous SFPQ or PSPC1 with
280 endogenous NONO using the same NONO antibody as used for biochemical assays. To the
281 best of our knowledge, however, there are currently no suitable and validated SFPQ or PSPC1
282 antibodies available that would allow co-staining with this NONO antibody. Thus, we
283 ectopically expressed full length, HA-tagged NONO (HA-NONO), in U2OS. As expected, HA-
284 NONO localized to the nucleoplasm in unperturbed cells and displayed a more pan-nuclear
285 localization upon etoposide treatment (Fig. S3A). A fraction of HA-NONO also accumulated
286 in the nucleolus, as monitored by partial co-localization with the nucleolar marker fibrillarin
287 (Fig. S3B). Importantly, treatment with etoposide did not alter the expression levels of HA-
288 NONO (Fig. S3C). Next, we co-stained endogenous DBHS proteins with HA-NONO.
289 Reassuringly, HA antibody reactivity displayed strong co-localization with each of the three
290 DBHS family members irrespective of etoposide treatment (Fig. 3A and B). Moreover, pan-
291 nuclear localization could be observed for a fraction of both HA-NONO, and each of the three
292 endogenous DBHS proteins in response to etoposide treatment. We conclude that NONO

293 associates with SFPQ and PSCP1 *in vivo* and that the bulk of these associations is resistant to
294 etoposide treatment.
295
296 **DISCUSSION**
297 Our study compared NONO protein interactions in the absence or presence of DNA damage.
298 Our mass spectrometry data confirmed the interaction of NONO with DBHS family member,
299 which was further validated by co-immunoprecipitation assays and co-localization studies. The
300 interactome data further indicate that NONO associates with numerous other RBPs. However,
301 our approach did not reveal any clear change in NONO interactions upon induction of DSBs.
302 Albeit confirming stable, etoposide-resistant formation of dimers between NONO and other
303 DBHS family members, the interpretation of DNA damage-induced changes in NONO
304 interactions may suffer from limitations.
305 NONO shares more than 70 % of sequence homology with SFPQ and PSPC1. The
306 conserved DBHS region of NONO contains two RNA recognition motifs (RRM1 and RRM2),
307 a NONA/paraspeckle domain (NOPS), and a coiled-coil domain [8]. NONO also contains an
308 amino-terminal histidine proline glutamine (HPQ)-rich region and a carboxy-terminal
309 glutamine proline (GP)-rich region, which harbors a nuclear localization sequence (NLS). The
310 canonical RRM1 and non-canonical RRM2 facilitate the binding of NONO to various nucleic
311 acid substrates, whereas the dimerization of DBHS proteins relies on the interaction between
312 the RRM2 domain of one paralog with the NOPS and coiled-coil domains of the other paralog
313 [8,43]. Intriguingly, phosphoproteomic data suggest that the induction of DNA damage by
314 ionizing radiation alters phosphorylation at NONO at threonine residues T428 and T450, which
315 are located in the carboxy-terminal region of NONO [44]. It is tempting to speculate that NONO
316 also undergoes differential phosphorylation upon etoposide treatment and that DNA damage-
317 responsive post-translational modifications alter NONO protein-protein interactions. However,

318 NONO is a multifunctional RBPs and modulates numerous processes in the nucleus. Thus, the
319 fraction of NONO susceptible to DNA damage may be rather small and its analysis likely
320 requires the generation of more selective tools such as phospho-specific antibodies. Our
321 imaging data using a pan-NONO antibody indeed indicate that a minor fraction of the nuclear
322 NONO pool is responsive to etoposide treatment, at least for the conditions used in this study.
323 Typically, factors involved in the recognition and repair of DSBs accumulate at such lesions
324 and form foci that can be visualized by microscopy. However, we did not observe the formation
325 of NONO-positive foci. A selective phospho-specific NONO antibody may not only reveal the
326 formation of NONO-positive DSB foci, but also facilitate a refined analysis of the NONO
327 protein-protein interactome in response to DNA damage. The data set could further benefit from
328 improvements in the mass spectrometry protocol, such as immunoprecipitation from subcellular
329 fractions and the usage of orthogonal assays to study interactomes, such as proximity labelling
330 approaches. The latter allows profiling of proteins that localize in distinct subcellular
331 compartments including the nucleolus [45]. This may define changes in NONO protein-protein
332 interactions in the future.

333 Our data indicate that a subset of NONO accumulates in the nucleolus upon etoposide
334 treatment. However, NONO relocalization is not quantitative, and therefore potential changes
335 in NONO interactions upon DNA damage are difficult to resolve by mass spectrometry.
336 Interestingly, a more quantitative relocalization of NONO and other DBHS to the nucleolus has
337 been observed upon ionizing radiation [46]. Thus, DNA damage-induced changes in the NONO
338 interactome may occur concomitant with relocalization, for instance upon harsher treatment
339 conditions that induce more persistent DSBs and likely trigger a more comprehensive
340 engagement of NONO in DDR.

341 Overall, our study provides insights in the interactome of NONO in response to
342 etoposide treatment and suggests remarkable stability of the bulk of NONO protein-protein

343 interactions upon induction of DNA damage. It will be important to determine if the genome-
344 protective role of NONO occurs mostly in association with other DBHS family members or if
345 distinct types of DNA damage selectively engage individual DBHS protein family members in
346 DDR.
347

348 **DATA AVAILABILITY**

349 Proteomics data are available at the ProteomeXchange consortium via the PRIDE partner
350 repository [47] with the identifier PXD061274 (reviewer token: aFmB1YlDmtL1) or upon
351 login to the PRIDE website via reviewer account (username: reviewer_pxd061274@ebi.ac.uk,
352 password: 3Uo7pqlSPyJP).

353

354 **CONFLICT OF INTEREST**

355 The authors declare no conflict of interest.
356

357 **SUPPORTING INFORMATION**

358 **Figure S1.** Validation of NONO antibody selectivity in U2OS cells. (A, B) Immunoblot
359 detecting NONO in whole cell extracts (A) and confocal imaging of NONO (B) upon transient
360 transfection of siRNA targeting NONO (siNONO) or non-targeting control siRNA (siControl).
361 Vinculin, loading control; broken circle, nucleus. Representative images are shown. (C)
362 Quantitation of (B) using RGB profiler line scan analysis. a.u., arbitrary units. (D) Confocal
363 imaging of 53BP1 and γH2A.X foci. Representative images are shown. (E) Quantitation of (D)
364 using RGB profiler line scan analysis. (F) Immunoblot detecting NONO upon
365 immunoprecipitation (IP) with NONO antibody from whole cell lysates (IN, input). IgG,
366 isotype control antibody. (G) Immunoblot detecting NONO upon immunoprecipitation (IP)
367 with NONO antibody from whole cell lysates and native PAGE. Silver stain, loading control;

368 exp., exposure. Full blots are shown. (H) as in (G) but comparing NONO signals upon native
369 PAGE (left) and reducing PAGE (right). Full blots are shown. Control, non-crosslinked
370 condition, BS3, bis(sulfosuccinimidyl)suberate; DMP, dimethyl pimelimidate.
371
372 **Figure S2.** Quality control for NONO mass spectrometry in U2OS cells. (A) Coomassie stain
373 upon immunoprecipitation (IP) with NONO antibody from whole cell lysates. IgG, isotype
374 control antibody. (B) Correlation analysis of mass spectrometry replicates. Both the x-axis and
375 the y-axis display intensities of peptides. r, correlation coefficient. (C) Stratification of top30
376 mass spectrometry hits.
377
378 **Figure S3.** Quality control for ectopic expression of HA-tagged NONO in U2OS cells. (A)
379 Confocal imaging of HA-NONO upon transient transfection of pcDNA3.1-HA-NONO
380 expression plasmid. FBL, Fibrillarin, nucleolar marker. Representative images are shown. (B)
381 Quantitation of (A) using RGB profiler line scan analysis. a.u., arbitrary units. (C) Immunoblot
382 detecting HA-NONO upon transient transfection of pcDNA3.1-HA-NONO expression plasmid
383 in whole cell extracts. Vinculin, loading control; mock, non-transfected control.
384
385 **Figure S4.** Raw data. Uncropped immunoblots are shown. Red box, cropped area depicted in
386 figure panels.
387
388 **Table S1.** Mass spectrometry data.
389
390 **Table S2.** List of top100 mass spectrometry hits.
391
392 **ACKNOWLEDGMENTS**

We thank all members of the department for support. We acknowledge Lea Boten and Teresa Klugt for excellent technical assistance. This work was funded by a grant from the German Cancer Aid (grant code: 8606100-NG1) awarded to KB.

Author contributions: Conceptualization, BT, AS and KB; Methodology, BT, SL, AS and KB; Investigation, BT and KB; Formal Analysis, BT, SL, AS and KB; Writing – Original Draft, BT and KB; Writing – Review & Editing, AS and KB; Funding Acquisition, KB; Supervision, AS and KB.

REFERENCES

1. Gebauer F, Schwarzl T, Valcárcel J, Hentze MW. RNA-binding proteins in human genetic disease. Nat Rev Genet. 2021 Mar;22(3):185-198.

2. Corley M, Burns MC, Yeo GW. How RNA-Binding Proteins Interact with RNA: Molecules and Mechanisms. Mol Cell. 2020 Apr 2;78(1):9-29.

3. Fox AH, Nakagawa S, Hirose T, Bond CS. Paraspeckles: Where Long Noncoding RNA Meets Phase Separation. Trends Biochem Sci. 2018 Feb;43(2):124-135.

4. Bond CS, Fox AH. Paraspeckles: nuclear bodies built on long noncoding RNA. J Cell Biol. 2009 Sep 7;186(5):637-44.

5. Clemson CM, Hutchinson JN, Sara SA, Ensminger AW, Fox AH, Chess A, et al. An architectural role for a nuclear noncoding RNA: NEAT1 RNA is essential for the structure of paraspeckles. Mol Cell. 2009 Mar 27;33(6):717-26.

6. Hirose T, Virnicchi G, Tanigawa A, Naganuma T, Li R, Kimura H, et al. NEAT1 long noncoding RNA regulates transcription via protein sequestration within subnuclear bodies. Mol Biol Cell. 2014 Jan;25(1):169-83.

7. Sasaki YT, Ideue T, Sano M, Mituyama T, Hirose T. MENepsilon/beta noncoding RNAs are essential for structural integrity of nuclear paraspeckles. Proc Natl Acad Sci U S A. 2009 Feb 24;106(8):2525-30.

8. Knott GJ, Bond CS, Fox AH. The DBHS proteins SFPQ, NONO and PSPC1: a multipurpose molecular scaffold. Nucleic Acids Res. 2016 May 19;44(9):3989-4004.

9. Zhang Z, Carmichael GG. The fate of dsRNA in the nucleus: a p54(nrb)-containing complex mediates the nuclear retention of promiscuously A-to-I edited RNAs. Cell. 2001 Aug 24;106(4):465-75.

10. Prasanth KV, Prasanth SG, Xuan Z, Hearn S, Freier SM, Bennett CF, et al. Regulating gene expression through RNA nuclear retention. Cell. 2005 Oct 21;123(2):249-63.

426 11. Lewis BA, Das SK, Jha RK, Levens D. Self-assembly of promoter DNA and RNA Pol
427 II machinery into transcriptionally active biomolecular condensates. Sci Adv. 2023 Oct
428 20;9(42):eadi4565.

429 12. Wei Y, Luo H, Yee PP, Zhang L, Liu Z, Zheng H, et al. Paraspeckle Protein NONO
430 Promotes TAZ Phase Separation in the Nucleus to Drive the Oncogenic Transcriptional
431 Program. Adv Sci (Weinh). 2021 Dec;8(24):e2102653.

432 13. Emili A, Shales M, McCracken S, Xie W, Tucker PW, Kobayashi R, et al. Splicing
433 and transcription-associated proteins PSF and p54nrb/nonO bind to the RNA polymerase II
434 CTD. RNA. 2002 Sep;8(9):1102-11.

435 14. Amelio AL, Miraglia LJ, Conkright JJ, Mercer BA, Batalov S, Cavett V, et al. A
436 coactivator trap identifies NONO (p54nrb) as a component of the cAMP-signaling
437 pathway. Proc Natl Acad Sci U S A. 2007 Dec 18;104(51):20314-9.

438 15. Mamontova V, Trifault B, Burger K. Nono induces Gadd45b to mediate DNA repair.
439 Life Sci Alliance. 2024 Jun 6;7(8):e202302555.

440 16. Kameoka S, Duque P, Konarska MM. p54(nrb) associates with the 5' splice site within
441 large transcription/splicing complexes. EMBO J. 2004 Apr 21;23(8):1782-91.

442 17. Peng R, Hawkins I, Link AJ, Patton JG. The splicing factor PSF is part of a large
443 complex that assembles in the absence of pre-mRNA and contains all five snRNPs. RNA
444 Biol. 2006 Apr;3(2):69-76.

445 18. Zhang S, Cooper JA, Chong YS, Naveed A, Mayoh C, Jayatilleke N, et al. NONO
446 enhances mRNA processing of super-enhancer-associated GATA2 and HAND2 genes in
447 neuroblastoma. EMBO Rep. 2022 Nov 23:e54977.

448 19. Ronchetti D, Traini V, Silvestris I, Fabbiano G, Passamonti F, Bolli N, et al. The
449 pleiotropic nature of NONO, a master regulator of essential biological pathways in cancers.
450 Cancer Gene Ther. 2024 Jul;31(7):984-994.

451 20. Hanahan D. Hallmarks of Cancer: New Dimensions. Cancer Discov. 2022
452 Jan;12(1):31-46.

453 21. Jackson SP, Bartek J. The DNA-damage response in human biology and disease.
454 Nature. 2009 Oct 22;461(7267):1071-8.

455 22. Ciccia A, Elledge SJ. The DNA damage response: making it safe to play with knives.
456 Mol Cell. 2010 Oct 22;40(2):179-204.

457 23. Blackford AN, Jackson SP. ATM, ATR, and DNA-PK: The Trinity at the Heart of the
458 DNA Damage Response. Mol Cell. 2017 Jun 15;66(6):801-817.

459 24. Zong D, Oberdoerffer P, Batista PJ, Nussenzweig A. RNA: a double-edged sword in
460 genome maintenance. Nat Rev Genet. 2020 Nov;21(11):651-670.

461 25. Burger K, Ketley RF, Gullerova M. Beyond the Trinity of ATM, ATR, and DNA-PK:
462 Multiple Kinases Shape the DNA Damage Response in Concert With RNA Metabolism.
463 Front Mol Biosci. 2019 Aug 2;6:61.

464 26. Feng P, Li L, Deng T, Liu Y, Ling N, Qiu S, et al. NONO and tumorigenesis: More
465 than splicing. J Cell Mol Med. 2020 Apr;24(8):4368-4376.

466 27. Bladen CL, Udayakumar D, Takeda Y, Dynan WS. Identification of the
467 polypyrimidine tract binding protein-associated splicing factor.p54(nrb) complex as a
468 candidate DNA double-strand break rejoining factor. J Biol Chem. 2005 Feb
469 18;280(7):5205-10.

470 28. Krietsch J, Caron MC, Gagné JP, Ethier C, Vignard J, Vincent M, et al. PARP
471 activation regulates the RNA-binding protein NONO in the DNA damage response to
472 DNA double-strand breaks. Nucleic Acids Res. 2012 Nov 1;40(20):10287-301.

473 29. Li S, Kuhne WW, Kulharya A, Hudson FZ, Ha K, Cao Z, et al. Involvement of
474 p54(nrb), a PSF partner protein, in DNA double-strand break repair and radioresistance.
475 Nucleic Acids Res. 2009 Nov;37(20):6746-53.

476 30. Kuhnert A, Schmidt U, Monajembashi S, Franke C, Schlott B, Grosse F, et al.
477 Proteomic identification of PSF and p54(nrb) as TopBP1-interacting proteins. J Cell
478 Biochem. 2012 May;113(5):1744-53.

479 31. Salton M, Lerenthal Y, Wang SY, Chen DJ, Shiloh Y. Involvement of Matrin 3 and
480 SFPQ/NONO in the DNA damage response. Cell Cycle. 2010 Apr 15;9(8):1568-76.

481 32. Fan XJ, Wang YL, Zhao WW, Bai SM, Ma Y, Yin XK, et al. NONO phase separation
482 enhances DNA damage repair by accelerating nuclear EGFR-induced DNA-PK activation.
483 Am J Cancer Res. 2021 Jun 15;11(6):2838-2852.

484 33. Yasuhara T, Xing YH, Bauer NC, Lee L, Dong R, Yadav T, et al. Condensates
485 induced by transcription inhibition localize active chromatin to nucleoli. Mol Cell. 2022
486 Aug 4;82(15):2738-2753.e6.

487 34. Trifault B, Mamontova V, Cossa G, Ganskih S, Wei Y, Hofstetter J, et al. Nucleolar
488 detention of NONO shields DNA double-strand breaks from aberrant transcripts. Nucleic
489 Acids Res. 2024 Apr 12;52(6):3050-3068.

490 35. Hu SB, Xiang JF, Li X, Xu Y, Xue W, Huang M, et al. Protein arginine
491 methyltransferase CARM1 attenuates the paraspeckle-mediated nuclear retention of
492 mRNAs containing IRAlus. Genes Dev. 2015 Mar 15;29(6):630-45.

493 36. Cui Y, Xie R, Zhang X, Liu Y, Hu Y, Li Y, et al. OGA is associated with
494 deglycosylation of NONO and the KU complex during DNA damage repair. Cell Death
495 Dis. 2021 Jun 16;12(7):622.

496 37. Deshar R, Yoo W, Cho EB, Kim S, Yoon JB. RNF8 mediates NONO degradation
497 following UV-induced DNA damage to properly terminate ATR-CHK1 checkpoint
498 signaling. Nucleic Acids Res. 2019 Jan 25;47(2):762-778.

499 38. Cox J, Mann M. MaxQuant enables high peptide identification rates, individualized
500 p.p.b.-range mass accuracies and proteome-wide protein quantification. Nat Biotechnol.
501 2008 Dec;26(12):1367-72.

502 39. Cox J, Hein MY, Luber CA, Paron I, Nagaraj N, Mann M. Accurate proteome-wide
503 label-free quantification by delayed normalization and maximal peptide ratio extraction,
504 termed MaxLFQ. Mol Cell Proteomics. 2014 Sep;13(9):2513-26.

505 40. Naganuma T, Nakagawa S, Tanigawa A, Sasaki YF, Goshima N, Hirose T.
506 Alternative 3'-end processing of long noncoding RNA initiates construction of nuclear
507 paraspeckles. EMBO J. 2012 Oct 17;31(20):4020-34.

508 41. West JA, Davis CP, Sunwoo H, Simon MD, Sadreyev RI, Wang PI, et al. The long
509 noncoding RNAs NEAT1 and MALAT1 bind active chromatin sites. Mol Cell. 2014 Sep
510 4;55(5):791-802.

511 42. Trifault B, Mamontova V, Burger K. In vivo Proximity Labeling of Nuclear and
512 Nucleolar Proteins by a Stably Expressed, DNA Damage-Responsive NONO-APEX2
513 Fusion Protein. Front Mol Biosci. 2022 Jun 6;9:914873.

514 43. Knott GJ, Chong YS, Passon DM, Liang XH, Deplazes E, Conte MR, et al. Structural
515 basis of dimerization and nucleic acid binding of human DBHS proteins NONO and
516 PSPC1. Nucleic Acids Res. 2022 Jan 11;50(1):522-535.

517 44. Beli P, Lukashchuk N, Wagner SA, Weinert BT, Olsen JV, Baskcomb L, et al.
518 Proteomic investigations reveal a role for RNA processing factor THRAP3 in the DNA
519 damage response. Mol Cell. 2012 Apr 27;46(2):212-25.

520 45. Hung V, Udeshi ND, Lam SS, Loh KH, Cox KJ, Pedram K, et al. Spatially resolved
521 proteomic mapping in living cells with the engineered peroxidase APEX2. Nat Protoc.
522 2016 Mar;11(3):456-75.

523 46. Moore HM, Bai B, Boisvert FM, Latonen L, Rantanen V, Simpson JC, et al.
524 Quantitative proteomics and dynamic imaging of the nucleolus reveal distinct responses to
525 UV and ionizing radiation. Mol Cell Proteomics. 2011 Oct;10(10):M111.009241.

526 47. Vizcaíno JA, Côté RG, Csordas A, Dianes JA, Fabregat A, Foster JM, et al. The
527 PRoteomics IDEntifications (PRIDE) database and associated tools: status in 2013. Nucleic
528 Acids Res. 2013 Jan;41(Database issue):D1063-9.

529

530 **FIGURE LEGENDS**

531 **Figure 1. Assessment of NONO interactomes in U2OS cells.** (A) Intensity versus ratio plots
532 displaying NONO mass spectrometry hits. 238 proteins that were detected with at least five
533 unique peptides identified by mass spectrometry are shown. Data are normalized to IgG isotype
534 controls and represent two merged biological replicates. The x-axis/y-axis displays
535 ratios/intensities of peptides. The number of unique peptides correlates with the size of each
536 circle and the significance is color-coded. (B, C) Immunoblots detecting NONO, PSPC1 and

537 SFPQ in whole cell extracts (IN, input) and upon immunoprecipitation (IP) with NONO
538 antibody (B) or SFPQ antibody (C). IgG, isotype control; Ki-67, negative control. (D) Venn
539 diagram showing overlap of NONO mass spectrometry hits. The top100 proteins have been
540 assessed.
541
542 **Figure 2. Comparative analysis of NONO mass spectrometry hits in U2OS cells.** (A)
543 Integration of mass spectrometry conditions by ratio versus ratio depiction. 49 proteins that
544 were detected with at least five unique peptides identified by mass spectrometry and that were
545 at least 4-fold enriched over IgG isotype controls are shown. Data represent two merged
546 biological replicates. Both the x-axis and the y-axis display ratios of peptides, whilst the
547 diagonal axis displays intensities. The number of unique peptides correlates with the size of
548 each circle and the significance is color-coded. Green box, nuclear protein; grey box, non-
549 significant hits. (B) Table summarizing mass spectrometry data for top30 proteins in the
550 absence or presence of etoposide.
551
552 **Figure 3. Assessment of DBHS protein localization in U2OS cells.** (A) Confocal imaging of
553 either NONO (left), SFPQ (middle) or PSPC1 (right) in combination with HA-NONO upon
554 transient transfection of pcDNA3.1-HA-NONO expression plasmid. Representative images are
555 shown. (B) Quantitation of (A) using RGB profiler line scan analysis. a.u., arbitrary units.

Figure 1

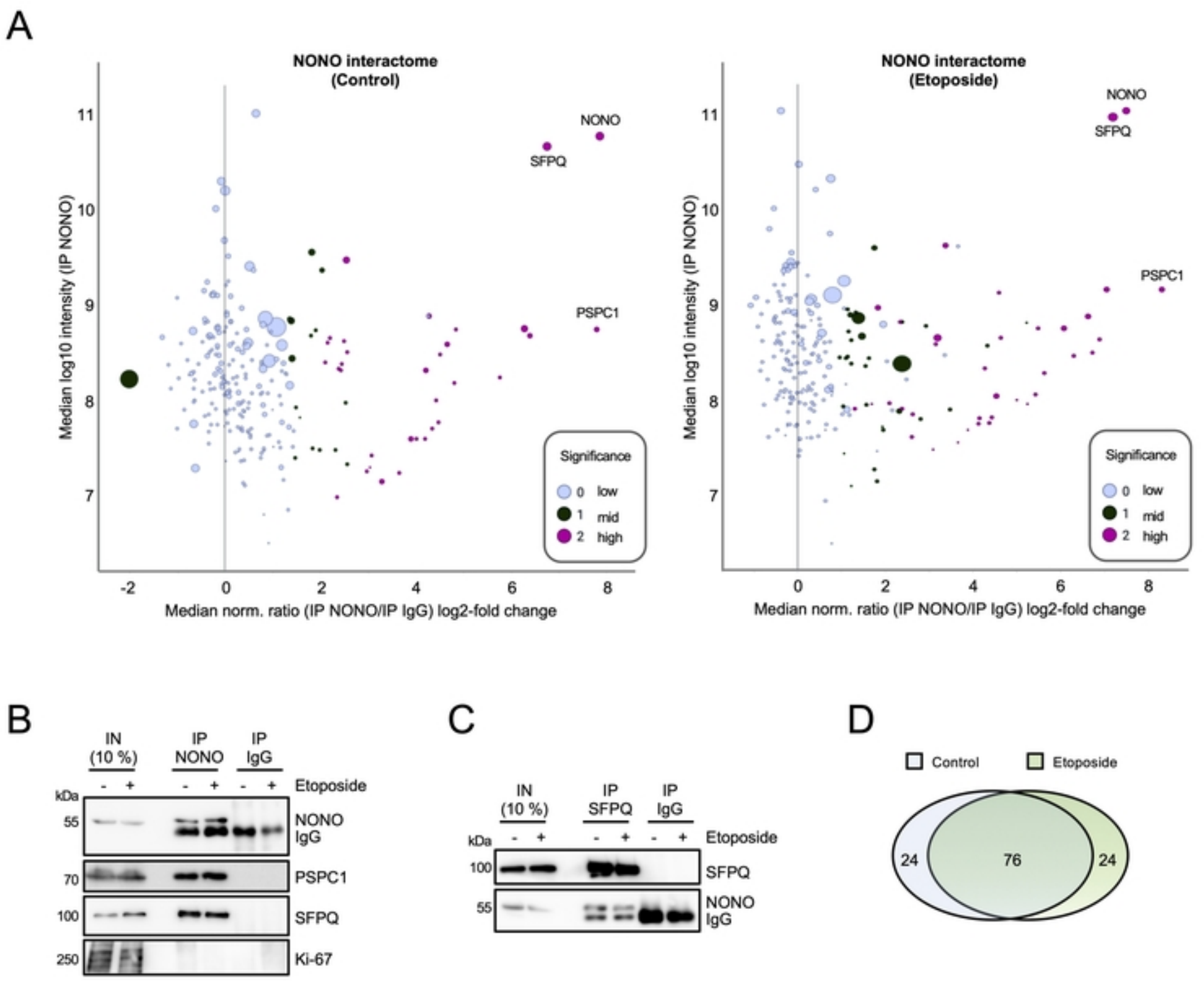

Figure_1

Figure 2

A

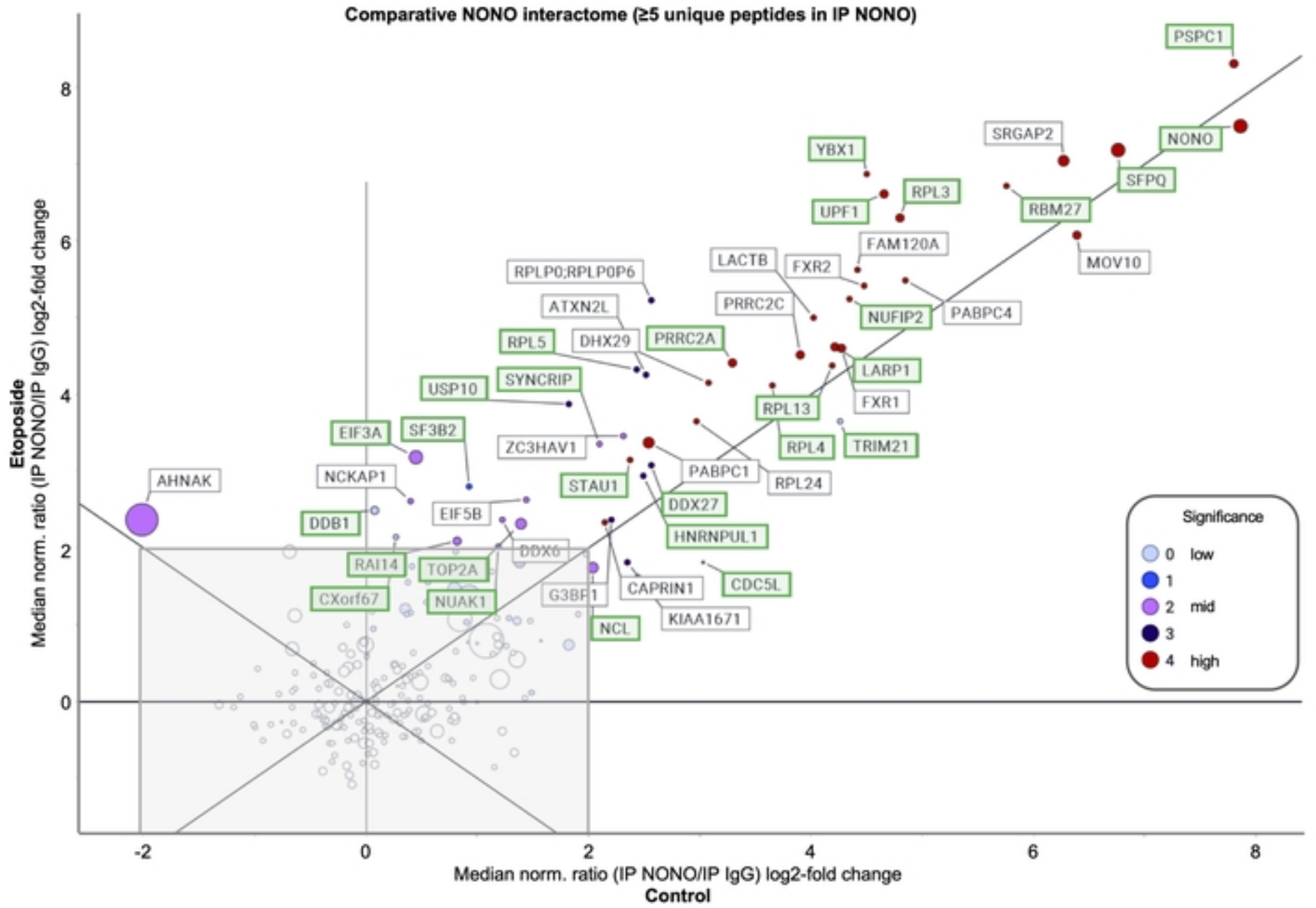

B

Rank	Gene	Average number of unique peptides		Average sequence coverage in %		Fold-enrichment (IP NONO / IP IgG)
		IP IgG	IP NONO	IP IgG	IP NONO	
1	NONO	13.0	62.0	28.5	70.4	231.7
	PSPC1	1.5	20.5	3.2	34.8	221.9
	SFPQ	19.0	63.0	28.7	58.3	107.8
	MOV10	7.0	27.5	8.2	28.5	83.5
	SRGAP2	6.0	30.0	6.4	31.6	76.9
	RBM27	0.0	17.0	0.0	17.0	54.1
	PABPC4	7.5	18.5	21.9	35.5	28.6
	RPL3	5.0	16.5	12.4	34.3	27.9
	UPF1	11.0	28.5	11.9	29.1	25.2
10	YBX1	3.5	7.5	33.4	44.5	22.7
	FXR2	0.5	8.5	4.0	21.5	22.2
	FAM120A	3.5	14.5	4.3	18.5	21.4
	NUFIP2	1.5	8.0	2.7	14.3	20.3
	FXR1	4.5	17.5	12.7	30.3	19.3
	TRIM21	14.0	26.5	24.5	42.3	19.2
	LARP1	4.0	15.5	4.7	17.2	18.6
	RPL13	2.0	7.5	11.4	26.8	18.3
	LACTB	0.5	9.0	1.0	15.3	16.2
	PRRC2C	2.0	16.0	1.1	7.6	14.9
20	RPL4	3.5	6.5	7.4	13.9	12.5
	PRRC2A	1.5	14.5	1.3	10.6	9.8
	DHX29	2.0	10.5	2.3	9.2	8.4
	CDC5L	3.5	7.5	5.6	12.6	8.2
	RPL24	0.0	6.0	0.0	32.2	7.8
	RPLP0; RPLP0P6	6.5	6.5	23.7	23.2	5.9
	DDX27	4.0	7.5	6.0	10.7	5.9
	PABPC1	13.5	25.5	30.7	44.5	5.8
	ATXN2L	6.5	12.5	8.1	16.2	5.7
	HNRNPUL1	12.5	17.0	17.3	22.9	5.6
30	RBM14	7.5	13.0	15.3	21.7	5.4

Control

Gene	Average number of unique peptides		Average sequence coverage in %		Fold-enrichment (IP NONO / IP IgG)
	IP IgG	IP NONO	IP IgG	IP NONO	
PSPC1	0.5	31.5	1.0	43.5	317.1
NONO	13.0	68.5	24.9	77.0	179.4
SFPQ	8.5	72.5	14.2	62.4	145.7
SRGAP2	2.5	46.5	2.4	46.1	132.5
YBX1	0.5	12.5	1.4	55.0	117.5
RBM27	0.5	23.0	0.5	22.2	105.2
UPF1	2.0	38.5	2.0	38.0	97.9
RPL3	1.5	23.5	3.9	45.6	78.7
MOV10	3.0	39.0	3.1	40.6	67.7
FAM120A	0.5	24.5	0.8	27.6	49.3
PABPC4	2.0	18.0	8.1	37.5	44.6
FXR2	0.0	14.0	1.2	31.6	42.9
NUFIP2	1.0	10.5	1.9	16.4	37.7
RPLP0; RPLP0P6	3.0	10.0	14.9	30.5	37.3
LACTB	0.5	12.5	1.0	20.1	31.9
LARP1	4.0	26.0	4.2	28.8	24.6
FXR1	3.0	20.0	6.6	33.3	24.3
PRRC2C	0.0	30.0	0.0	12.5	23.0
PRRC2A	0.0	19.5	0.0	13.9	21.4
RPL13	1.0	13.0	5.7	43.1	20.8
RPL5	3.0	21.0	11.6	49.4	20.1
ATXN2L	2.5	19.0	2.6	23.2	19.1
DHX29	0.5	19.5	0.5	18.4	17.8
RPL4	0.0	16.0	0.0	31.4	17.4
USP10	0.5	10.5	0.8	15.5	14.7
TRIM21	16.0	28.5	27.5	46.1	12.6
RPL24	0.5	8.0	2.9	47.5	13.0
ZC3HAV1	1.5	13.0	2.3	17.4	11.0
PABPC1	9.0	25.5	18.9	48.5	10.3
SYNCRIP	1.5	8.0	6.4	21.5	10.2

Etoposide

Figure_2

Figure 3

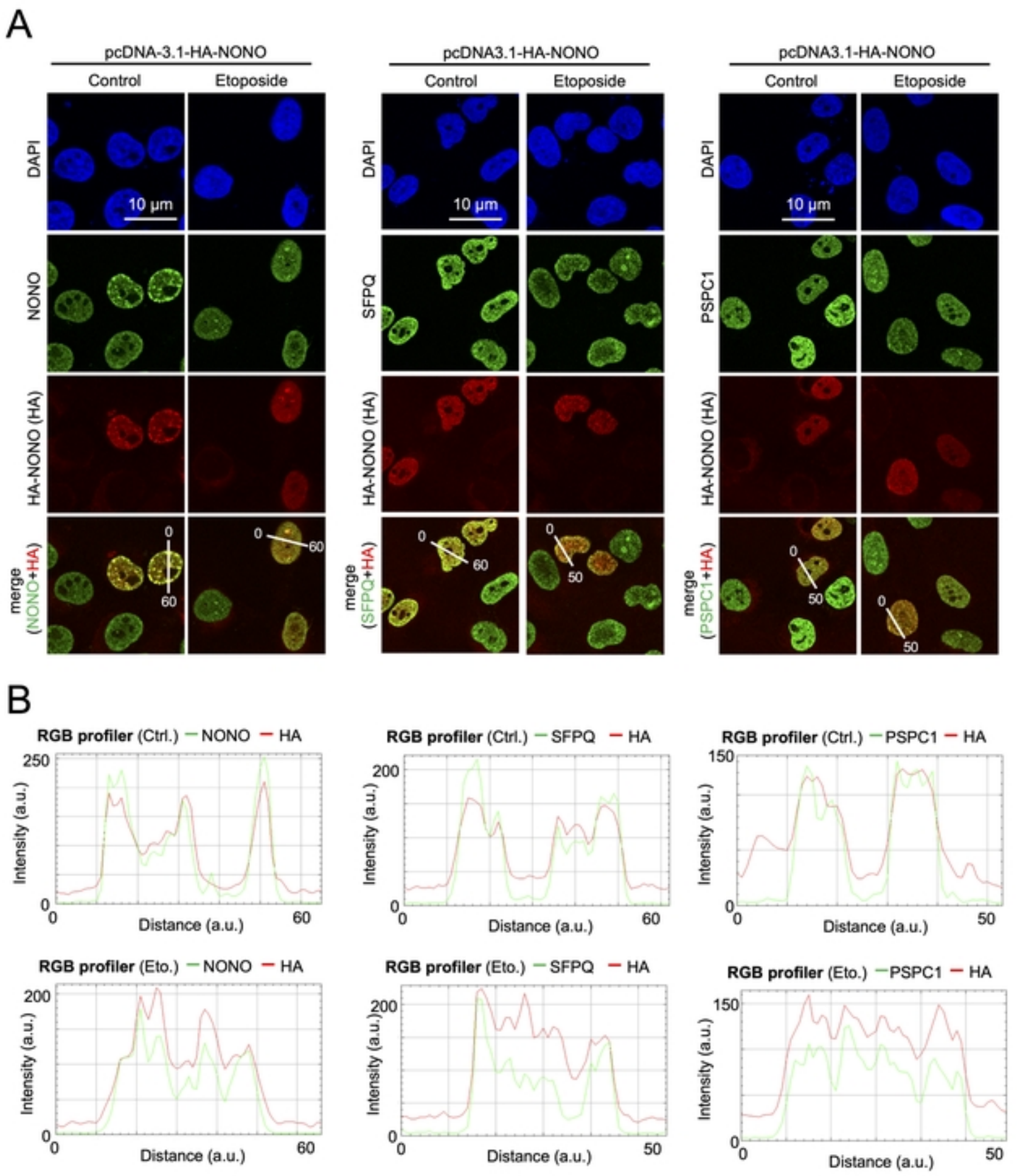

Figure_3